$ScVO_4$ under Non-Hydrostatic Compression: A New Metastable Polymorph

Alka B. Garg[*1], D. Errandonea[2], P. Rodríguez-Hernández[3], and A. Muñoz[3]

[1]High Pressure and Synchrotron Radiation Physics Division, Bhabha Atomic Research Centre, Mumbai 400085, India

[2]Departamento de Física Aplicada-ICMUV, MALTA Consolider Team, Universidad de Valencia, Edificio de Investigación, C/Dr. Moliner 50, Burjassot, 46100 Valencia, Spain

[3]Departamento de Física, Instituto de Materiales y Nanotecnología, MALTA Consolider Team, Universidad de La Laguna, La Laguna, E-38205 Tenerife, Spain

Abstract

The high-pressure behaviour of scandium vanadate ($ScVO_4$) is investigated under non-hydrostatic compression. The compound is studied by means of synchrotron based powder x-ray diffraction and optical absorption. The occurrence of a non-reversible phase transition is detected. The transition is from the zircon structure to a fergusonite-type structure and takes place around 6 GPa with nearly a 10% volume discontinuity. X-ray diffraction measurements on a pressure cycled sample confirm, for the first time, that fergusonite-type $ScVO_4$ can be recovered as a metastable phase at ambient conditions. Raman spectroscopic measurements verify the metastable phase to be fergusonite-type. Theoretical calculations also corroborate the experimental findings. The fergusonite phase is found to be stiffer than the ambient-pressure zircon phase as indicated by the observed experimental and theoretical bulk moduli. The optical properties and lattice-dynamics calculation of fergusonite $ScVO_4$ are discussed. At ambient pressure the band gap of zircon (fergusonite)-type $ScVO_4$ is 2.75 eV (2.3 eV). This fact suggests that the novel metastable polymorph of $ScVO_4$ can have applications in green technologies; for instance it can be used as photocatalytic material for hydrogen production by water splitting.

*Corresponding author, Email: alkagarg@barc.gov.in

Keywords: fergusonite, x-ray diffraction, optical absorption, high pressure, phase transition, equation of state

Introduction

$ScVO_4$ is the first and the lightest compound in the series of rare-earth (RE) orthovanadates, RVO_4 (R = Sc, Y, La-Lu). Due to their interesting optical properties these compounds have recently been investigated both theoretically and experimentally in the search for novel inorganic materials to be used in photonic industries. Indeed some of these materials have the potential to be employed as photocatalysts [1-3], polarizers [4,5], phosphors [6-8], scintillators for γ-ray detection [9,10], multiphoton-induced fluorescence materials [11], and nonlinear optical materials [12,13]. The doping of these materials with RE cations makes them extremely useful as laser materials. In fact, YVO_4, the mineral Wakefieldite, is one of the most widely used materials in the laser industry [14-16]. At ambient pressure and temperature most RE orthovanadates crystallize in tetragonal zircon-type structure with space group $I4_1/amd$. The basic building block of this structure is a chain of alternating edge-sharing VO_4 tetrahedra and RO_8 polyhedra running parallel to the c axis. The conventional unit cell has four formula units. The R^{+3} cations retain much of the non-interacting ionic character in these crystals.

At low temperature many RE orthovanadates undergo phase transitions from a high-symmetry tetragonal to a low-symmetry structure due to the cooperative Jahn-Teller effect [17]. Apart from various studies at ambient pressure and low temperature, a lot more of attention has been paid to the high-pressure (HP) investigation of these materials. Synchrotron based x-ray diffraction (XRD), Raman spectroscopic, and first principles calculations have established beyond doubt the zircon to scheelite phase transition in the RVO_4 compounds that contains RE elements with the smaller cationic radii (Sm-Lu) [18-26]. The transition is accompanied by a volume discontinuity of ≈ 10% and takes place at pressures below 10 GPa [18-26]. In the scheelite structure (space group $I4_1/a$), the V atoms and RE elements have the same coordination polyhedron that in the zircon structure. The

structural relations between both structures have been widely discussed in the literature [27]. On further compression, many of the RE orthovanadates undergo a second phase transition to a monoclinic fergusonite structure (space group *I*2/*a*). This structure is a monoclinic distortion of the schelite structure. It can be obtained by inducing a small movement of the RE and V atoms and larger displacements of the oxygens [28]. However, the fergusonite structure still has the same kind of polyhedral units than zircon and scheelite. Interestingly, there is a group–subgroup relationship ($I4_1/amd \rightarrow I4_1/a \rightarrow I2/a$) involved in the zircon-scheelite-fergusonite structural sequence. In the case of RVO_4 compounds with RE elements with the larger cationic radii (La-Nd), previous studies have shown that under compression they transform from the zircon to the monazite-type monoclinic structure (space group $P2_1/n$). This transition involves an increase in coordination number around the R^{+3} cation [29-34]. The HP phases of all RE orthovanadates are known to have band gaps smaller than the ambient-pressure zircon-type phases. The possibility to recover the HP phases, with band gaps close to 2 eV [35], as metastable phases at ambient conditions, make them more suitable than the ambient-pressure zircon phase for the development of green technologies, i.e. it can be used as photocatalytic material for hydrogen production by water splitting using sunlight [36].

Most of the HP investigations which have been reported on these materials so far have been carried out under hydrostatic/quasi-hydrostatic compression. However, in an earlier study on $HoVO_4$, we have reported that non-hydrostatic stresses trigger the transition to the fergusonite phase at much lower pressure than hydrostatic/quasi-hydrostatic compression [20]. Non-hydrostatic stresses are known to affect the crystal structure, phase transition sequence, transition pressure and the metastability of HP phases [37, 38]. Thus, we decided to use a new approach for investigating the possibility of synthesizing the metastable fergusonite-type phase of $ScVO_4$ using non-hydrostatic compression. We studied $ScVO_4$ up

to nearly 33GPa with synchrotron based powder XRD and successfully synthesized the metastable fergusonite phase. This was confirmed by optical-absorption and Raman spectroscopic measurements. The experimental findings were well supported by first-principles calculations. We determined the crystal structure, Raman and infrared (IR) phonons, and band gap of the metastable fergusonite-type polymorph of $ScVO_4$.

Experimental Details

The samples used in the different experiments were obtained from polycrystalline $ScVO_4$. This compound was prepared by ceramic route. As precursor materials of the reaction, we used stoichiometric amounts of high-purity Sc_2O_3 (Alfa Aesar99.9%) and V_2O_5 (Aldrich 99.6%) powders. In the first step, in order to remove moisture or any other organic impurity from both oxides, they were heated separately and simultaneously at 425 K during a period of 24 hrs. In the second step, the mixture of Sc_2O_3 and V_2O_5 powders was meticulously ground for two hours using an agate mortar and pestle. In the third step, pellets (12.5 mm diameter and 5 mm thickness) were prepared by cold pressing the obtained mixture of powders. Subsequently, the pellets were heated at 1075 K in a furnace for 24 hrs and finally cooled to room temperature (RT). The synthesized material was characterized by powder XRD using rotating anode generator (RAG) with molybdenum anode (λ=0.7107 Å) and MAR345 image plate area detector. This measurement confirmed the single phase formation of zircon type $ScVO_4$ with unit-cell parameters determined at ambient conditions as a = 6.8000(6) Å and c = 6.1529(11) Å. These values are in close match with the values reported in the literature [39].

High-pressure XRD (HP-XRD) experiments were performed at room temperature up to 32.3 GPa. A diamond-anvil cell (DAC) with a large angular opening was used for pressure generation. The DAC was equipped with two diamond anvils with culets of 400 μm in

diameter. The pressure chamber for the sample was a 150 μm diameter hole drilled in a hardened stainless-steel gasket which was pre-indented to a thickness of 60 μm. In order to generate non-hydrostatic conditions, the experiments were carried out without using any pressure-transmitting medium. The $ScVO_4$ sample was loaded in the pressure chamber of the DAC together with few fine grains of platinum (Pt) which served as pressure standard. The pressure was determined with an accuracy of 0.1GPa using the equation of state (EOS) of Pt [40]. HP-XRD measurements were carried out in situ at the powder-diffraction station (XRD1 beamline) of the synchrotron source Elettra. The experiments were performed in an angle-dispersive geometry using monochromatic x-rays (λ = 0.5997 Å). The size of the x-ray beam was constrained using a circular collimator to a circular area of 80 μm in diameter. The XRD data were collected on a MAR345 image plate detector. Exposure times of 15–20 minutes were employed to acquire each of the XRD patterns we measured. The recorded two-dimensional diffraction images were integrated into standard one dimensional intensity versus two-theta profiles using the FIT2D software [41]. In order to determine the sample to detector distance and to calibrate the detector parameters a standard powder diffraction pattern of CeO_2 was used.

The structural refinement of the different polymorphs of $ScVO_4$ was carried out using GSAS [42]. The Rietveld refinements were performed following the procedure described next. The background of the XRD pattern was fitted with a Chebyshev polynomial function of first kind where six to eight coefficients were used. The shape of Bragg peaks was modelled using a pseudo-Voigt function. On the other hand, the site occupancy factor (SOF) and the overall displacement factor (B) were constrained for all atoms to SOF = 1 and B = 0.025 $Å^2$. We assume this approach, which usually works well for HP-XRD data, to reduce the number of free parameters used in the refinements [43]. In a first step, we determined only the unit-cell parameters by means of the Le-Bail extraction method as implemented in

GSAS [42]. The subsequent step was to Rietveld refine the unit-cell parameters by fixing the atomic positions to the literature values or to the values determined from calculations. This was followed by the refinement of atomic positional parameters by fixing the unit-cell parameters. Finally a full refinement was carried out in which all the crystal-structure parameters were simultaneously refined. For the diffraction data collected at a few pressure points a multiphase refinement was required. In such cases, independent peaks were carefully selected to determine the initial values of the relative scale factors. An iterative procedure was then carried out, fitting alternatively the parameters of the different phases until reaching small goodness of fit factors and a satisfactory fitting profile.

Raman spectroscopic and optical-absorption studies were performed using a Boehler-Almax DAC which was equipped with diamonds having 300 μm diameter culets. The sample loading procedure for these measurements was similar to the one described above for XRD measurements. In the Raman and optical experiments, the pressure was determined using the ruby scale [44] with an accuracy of 0.1GPa. Raman spectroscopic measurements were carried out in backscattering geometry. For the Raman set-up we used a Jobin−Yvon single spectrometer equipped with an edge filter and a thermoelectric-cooled multichannel CCD detector. The measurements were performed using the 514.5 nm line of an Ar^+-ion laser with a power of 20 mW. The laser was not absorbed by the sample then temperature effects can be neglected. The set-up was calibrated using the plasma lines of the laser. The spectral resolution of the Raman system was below 2 cm^{-1}. The optical-absorption measurements were made in the visible–near-IR range. They were carried out with a home-made set-up consisting of a tungsten lamp, fused silica lenses, reflecting optics objectives and an Ocean Optics visible–near-IR spectrometer [45]. The transmittance spectra of the sample were recorded using the sample-in sample-out method [46]. From the transmittance of the samples we determined the optical-absorption spectra at different pressures.

Details of Calculations

First-principles based simulations of the different physical properties of the two polymorphs of $ScVO_4$ were performed within the framework of density-functional theory (DFT) [47]. All calculations were carried out using the Vienna Ab initio simulation package (VASP) [48]. They were performed employing the projector augmented wave (PAW) method [49]. The full nodal character of the all-electron charge-density distribution in the core region was taken into account. Due to the presence of oxygen atoms, in order to obtain highly converged results and an accurate description of the electronic properties, a cut off of 520 eV was assumed for the kinetic energy. For the exchange-correlation energy, the generalized-gradient approximation (GGA) was assumed. In particular, we used the Perdew-Burke-Ernzenhof prescription for solids (PBEsol) [50]. Integrations over the Brillouin zone (BZ) were carried out using dense meshes of Monkhorst-Pack k-special points [51]. We used a 4×4×6 mesh for the zircon structure and 6×4×8 mesh for the fergusonite structure. The convergence achieved in the energy was better than 1 meV per formula unit. From the calculations we obtained the structural parameters at ambient pressure and as a function of pressure as well as the equilibrium volume, the total energy and enthalpy, the bulk modulus, and its pressure derivatives.

The relative stability of the different crystal structures was deduced by comparing their enthalpy as a function of pressure. Previous studies have shown that under hydrostatic conditions the fergusonite structure once relaxed systematically reduces to the scheelite structure [52]. In our case, in order to simulate non-hydrostatic conditions, a uniaxial stress was imposed to the studied structures. This allows the comparison with experimental studies carried out under non-hydrostatic conditions.

Lattice-dynamics calculations were performed at the zone centre (Γ point) of the BZ employing the direct method [53]. These calculations allow studying the different vibrational

modes at ambient and high pressure. They also let identifying the eigen vectors and symmetry of all the vibrational modes at the Γ point. Finally, electronic band-structure calculations were performed within the first BZ along high-symmetry directions. These calculations were carried out for the zircon and fergusonite structures. They were performed at ambient pressure and as a function of pressure for both polymorphs.

Results and Discussion

Figure 1(a) & (b) shows XRD patterns measured on $ScVO_4$ during pressure increase while figure 1(c) depicts patterns collected during pressure unloading. Diffraction peaks from platinum (in situ pressure standard) are marked as Pt. A weak reflection observed from the sample chamber is marked with an asterisk. The rest of the observed Bragg peaks at 0.5 GPa can be undoubtedly assigned to the ambient-pressure zircon phase as shown by the Rietveld refinement of the diffraction pattern in figure 2 (a). The various R-factors obtained from the refinement are R_p = 3.34 %, R_{wp} = 4.68 %, and R_F^2 = 4.14 % indicating the good quality of the refinement. The unit-cell parameters determined at 0.5 GPa are a = 6.7805(5) Å and c = 6.1522(12) Å. In the zircon structure, the positions of Sc and V atoms are fixed by symmetry; the Wyckoff positions are 4a and 4b respectively. The refined oxygen positions are given in table 1. In the XRD pattern collected at 3 GPa, the peaks from the sample show a slight broadening and (112) and (211) peaks merge into a single peak. This observation is not surprising as the presence of non-hydrostatic stresses results in broadening of XRD peaks [37, 38]. However, the XRD pattern could still be well fitted with the zircon structure. On further increasing the pressure until 5.7 GPa, no noticeable changes are observed except the overall shifting of the patterns to higher angles due to lattice compression. In the pattern collected at 6.5 GPa, a weak peak shown by an arrow in figure 1(a) appears on the right of the (200) peak of zircon, at the two theta value of ≈ 11.7°. There is also another peak appearing at low angles which is also indicated by an arrow. Less noticeable changes occur

near the (312) of the zircon structure. When the pressure is raised further, the peaks corresponding to the zircon phase gradually starts losing their intensity and the new peaks pick up in intensity. These observations indicate the occurrence of a pressure-induced structural change in the compound. This trend continues till 21 GPa. Beyond this pressure, the intensity of the Bragg peaks of the zircon phase reduces below the detectable limit of the experimental setup. Our observations imply a large pressure range of co-existence of the ambient- and high-pressure phases of $ScVO_4$. On further compressing the sample till 32.3 GPa, the highest pressure reached in the present investigations, no additional noticeable changes are observed in the XRD pattern except for the usual lattice compression. On releasing the pressure to ambient pressure, the XRD pattern resembles with that of the pattern at the highest pressure except that the peaks have shifted to lower angle. Then, apparently the phase transition is non-reversible.

To fit the crystal structure of HP phase, we tried with a pattern where there are no peaks from the zircon phase, which was collected at 25.6 GPa. The modeling of this pattern with the earlier reported high-pressure scheelite structure (space group $I4_1/a$, obtained under hydrostatic compression) could not explain the weak peaks at 2θ = 6.78º, 7.88º, and 8.14º. Then the next possible candidate which is fergusonite (space group $I2/a$) was tried to fit the data. It is worth mentioning here that the peak observed at 6.78º, which is indexed as the (020) reflection in fergusonite phase, is a fingerprint of this monoclinic structure. The Rietveld refinement achieved with the fergusonite structure at 25.6 GPa is shown in figure 2(b).The R-factors obtained from the refinement are R_p = 1.69%, R_{wp} = 2.32 %, and R_F^2 = 2.07%. The refined lattice parameters for the fergusonite phase at this pressure are a = 4.676(4)Å, b = 10.131(5)Å, c = 4.868(4)Å, β = 96.46(5)°. The refined atomic positions are given in table 1. All the XRD patterns measured from 25.6 GPa to 32.2 GPa can be properly refined with the fergusonite structure. The refined XRD pattern at 32.2 GPa pressure is

shown in figure 2(c). The lattice parameters extracted from the refinement are a = 4.650(4) Å, b =10.038(5) Å, c = 4.8487(29) Å, β = 96.99(5)°. The R-factors of the refinement are R_p = 1.54 %, R_{wp} = 2.09%, R_F^2 = 1.96 %. Based upon the Rietveld refinements, we conclude that under non-hydrostatic conditions a direct zircon-fergusonite transition might be triggered without passing through the intermediate scheelite phase. As we will discuss latter, this conclusion is consistent with the results we obtained from optical absorption, Raman spectroscopic experiments, and calculations. We would like to note here, that the differences between the behaviour of $ScVO_4$ (zircon-fergusonite transition) and $HoVO_4$ (zircon-scheelite-fergusonite) [20] can be caused by the use of different pressure media, no pressure medium in the present experiment ($ScVO_4$) and 4:1 methanol-ethanol in the study of $HoVO_4$ [20]. As a consequence of it, deviatoric stresses are expected to be larger in the present study [54], which could be the cause of reducing the onset of the transition pressure to fergusonite and eliminating the scheelite structure from the structural sequence of $ScVO_4$.

The XRD patterns collected during decompression could be fitted only with the fergusonite structure. The lowest pressure at which the data is collected while unloading is 0.7 GPa. Therefore, the zircon-fergusonite transition appears to be non-reversible. For the XRD patterns where both zircon and HP phase are present, a multi-phase refinement has been carried out considering the zircon and fergusonite structures. From it we obtained the pressure dependence of the unit-cell parameters of both phases. The lattice parameters determined as a function of pressure are shown in figure 3. The inset in the figure depicts the variation of monoclinic angle β of fergusonite $ScVO_4$. This angle increases with pressure indicating a larger distortion in the fergusonite structure and then tends to stabilize. The experiments performed upon decompression show the reduction in the distortion to the fergsuonite structure within the experimental error. Experimental pressure-volume data are shown in figure 4. For the zircon phase, we obtained similar results as in previous studies

carried out using silicon oil as pressure-transmitting medium [26]. The agreement between experiments and calculations is good for zircon $ScVO_4$ (see figures 3 and 4). Regarding the fergusonite structure, a fitting with a third order Birch-Murnaghan EOS [55] to the pressure-volume data yields a value of the ambient-pressure bulk modulus B_0 as 208(7) GPa with its pressure derivative as 4.9(3). In previously reported high-pressure x-ray diffraction measurements carried out using silicon oil as pressure transmitting medium (which becomes non-hydrostatic beyond 6 GPa [56]) the Bragg peaks from the HP scheelite phase appears at 8.7 GPa with the region of co-existence extending up to 23.4 GPa [26]. The reported value of bulk modulus for HP scheelite phase is 210(12) GPa with a pressure derivative of the bulk modulus of 5.3(8). These values agree within error bars with the EOS parameters obtained for fergusonite $ScVO_4$ from the present studies. Thus, we can conclude that the scheelite and fergusonite phases have a similar compressibility. The volume collapse at the zircon-fergusonite phase transition is around 10% indicating the nature of the transition to be first order. Regarding the axial compression of fergusonite phase, it can be seen in figure 3 that the compression is non-linear at low-pressure, becoming nearly linear beyond 5 GPa. We also observed that the *b* axis is the most compressible axis, the *a* axis is the least compressible one, with the *c* axis having an intermediate compressibility. The numerical values of the linear compressibilities of the axes are: 7.4×10^{-3}, 2.98×10^{-3}, and $4.24\times10^{-3}GPa^{-1}$, respectively. Theory and experiments give a similar pressure dependence of the unit-cell axis. The agreement is also good for the strongly non-linear pressure dependence of the β angle (see inset of figure 3).

Since the lowest pressure at which the XRD pattern was collected while unloading at the Elettra synchrotron source is 0.7 GPa, to confirm the metastability of HP phase, an additional experiment was performed. Knowing from optical, Raman, and previous XRD experiments that the minimum pressure needed to obtain a pure fergusonite phase is 21 GPa,

in this experiment, the sample was compressed in a DAC to 25 GPa. This was followed by releasing the pressure slowly to ambient pressure. In this experiment the ruby scale was used for pressure calibration. An XRD pattern on the retrieved sample, which was recovered from the DAC, was collected using the Indus synchrotron source at Indore (India) with a wavelength of 0.6426 Å. The measured XRD pattern and the Rietveld refined profile are shown in figure 5. The R-factors obtained from this refinement are R_p = 1.20%, R_{wp} = 1.65 %, and R_F^2 = 1.48%. The extracted lattice parameters from the refinement are *a* = 4.8371(26) Å, *b* = 10.5557(4) Å, *c* = 4.9161(28) Å, and β = 91.603(23)°. The refined atomic coordinates are summarized in table 1.

Before discussing the rest of the results of our studies, we would like to mention here that the XRD technique used in our study is accurate enough for identifying the crystal structures but not to clarify the transition mechanism of the zircon-fergusonite transformation. In particular, to obtain information on the influence of local stress fields in the phase transition. Such information can be obtained from micro-Laue techniques which have been recently applied to elaborate the mechanism of zircon-scheelite phase transition in $GdVO_4$ [57]. Such studies will help to clarify why the intermediate scheelite phase is observed between zircon and fergusonite under hydrostatic conditions and why not under non hydrostatic conditions. However, micro-Laue diffraction is beyond the scope of the present work. We hope our results will contribute to trigger the application of this technique in the near future to explore the HP behaviour of $ScVO_4$ and in particular the zircon-fergusonite transition.

In the following paragraph we will describe the results from structural calculations. It is known that under hydrostatic conditions, DFT calculations agree with the experimental findings of HP zircon-scheelite transition [52]. However, in the present studies we found that deviatoric stresses can favour a zircon-fergusonite transition as shown in figure 6, where we

show the enthalpy versus pressure data. In particular, we found that a uniaxial stress of 1.2 GPa is sufficient to trigger the transition from zircon to fergusonite at 2.5 GPa. This pressure is smaller than the experimental onset pressure. The difference in the transition pressure can be due to the fact that calculations were carried out at 0 K temperature and experiments were performed at room temperature. Another possible cause of this small discrepancy could be due the presence of quantitatively unknown stress field in the experiments, which, does not match exactly with the simulated stress field in the calculations. However, calculations qualitatively confirm that non-hydrostaticity indeed could trigger a direct zircon-fergusonite transition. The difference in the transition pressure is consistent with the presence of large kinetic barriers which are typical of phase transitions that involve a large atomic rearrangement like the zircon-fergsuonite transition. This is also coherent with the large hysteresis associated to the transition which allows recovering the fergusonite phase as a metastable phase at ambient pressure after decompression. The calculated structural parameters (unit-cell parameters and atomic coordinates) at ambient pressure are given in table 2. They are in reasonable agreement with the parameters obtained from the refinement of experimental data. The evolution of lattice parameters and pressure volume data obtained from theory for both the zircon and fergusonite phases along with experimental data points are shown in figures 3 and 4 respectively. In both the figures, it can be seen that calculations agree very well with the experimental results for the zircon phase. For the fergusonite phase, the agreement is good regarding the changes induced by pressure in the unit-cell parameters and volume; however their absolute values are slightly underestimated. However, the theoretical underestimation lies within the typical reported systematic errors in DFT-GGA calculations. The origin of it can be related to the selection of exchange-correlation functionals. From the calculations, the ambient pressure bulk modulus and its pressure derivative for the fergusonite phase when fitted with a 3rd order Birch-Murnaghan EOS [55]

are B_0 = 187.78GPa and B_0' = 5.93. The calculated value of the bulk modulus fairly agrees with the experimental value.

The effect of pressure in the optical properties of $ScVO_4$ will be discussed in the following paragraph. The optical absorption of $ScVO_4$ at different pressures is shown in figure 7. At 0.2 GPa the absorption spectrum shows a steep absorption close to 2.8 eV, which corresponds to the fundamental absorption edge of a direct band gap that overlaps with a low-energy absorption tail. This tail has been previously observed in related compounds being related to the presence of defects [58]. However, its presence does not preclude the determination of the band-gap energy (E_g) which can be obtained using a Tauc-plot analysis [59]. For zircon-type $ScVO_4$ we determined E_g = 2.75(5) eV. This band gap is very similar to that of $BiVO_4$ [60] and it is in the middle of the values of E_g predicted for ambient pressure by previous calculations [61] (2.43 – 3.2 eV). We have carried out band-structure calculations for the low-pressure phase of $ScVO_4$. The results are shown in figure 8. Our results indicate that zircon-type $ScVO_4$ is a direct gap material with the maximum of the valence band and the minimum of the conduction band at the Γ point of the Brillouin zone. The calculated E_g at ambient pressure is 2.5 eV. The 0.25 eV underestimation of E_g, in comparison with experiments, is typical of DFT calculations [62]. From the calculated electronic density of states (figure 8) we determined that the upper part of the valence band consists of O 2p and V 3p states whereas the lowest part of the conduction band is dominated by V 3d and O 3p states with some contribution from Sc 3d states. Upon compression, both experiments and calculations indicate that pressure has little effect on the band structure of zircon-type $ScVO_4$. From figure 7 it can be seen that from 0.2 to 7.9 GPa the absorption spectrum only slightly blue shift. From the experiments and calculations we estimated $dE_g/dP \approx 1$ meV/GPa.

When compressing $ScVO_4$ under non-hydrostatic conditions we found that beyond 9 GPa $ScVO_4$ becomes yellowish. This occurs together with changes in the absorption

spectrum (see figure 7) which imply a sudden decrease of E_g to 2.3 eV. This fact is consistent with the observation of the zircon-fergusonite transition described above. After compression up to 30 GPa and decompression to ambient pressure, we determined from our sample a slightly higher band gap, E_g = 2.32 eV. This fact makes the new phase of $ScVO_4$ potentially useful as the photocatalytic material for hydrogen production. We have calculated the band structure and electronic density of states of fergusonite $ScVO_4$. According to calculations fergusonite $ScVO_4$ has a direct band gap at the Γ point of the Brillouin zone with E_g = 2.0 eV. This value is 0.3 eV smaller than the measured E_g. This underestimation of E_g by calculations in the fergusonite phase is similar to the underestimation of E_g by calculations in the zircon phase (0.25 eV). Regarding the band-gap collapse, calculations predicts a decrease of E_g from 2.5 (zircon) to 2.0 eV (fergusonite), which is fully consistent with our experimental observations (E_g changes 0.45 eV from 2.75 to 2.3 eV). Regarding the composition of the density of states (figure 9) in the fergusonite structure the upper part of the valence band consists mainly of O 2p states and the lowest part of the conduction band is dominated by V 3d with some contribution from O 3p and Sc 3d states. As for zircon phase, E_g for fergusonite phase is also slightly effected with pressure. However, in contrast with the behaviour of E_g in the low-pressure phase, in the HP fergusonite phase, E_g redshifts under compression. At ambient pressure E_g = 2.32 eV, at 9.2 GPa, E_g = 2.3 eV, and at 19.7 GPa E_g = 2.28 eV. Calculations predict a similar evolution of the band gap energy with pressure. The estimated dE_g/dP comes out to be ≈ -2meV/GPa.

A final confirmation of the metastability of the HP fergusonite phase comes from Raman spectroscopic measurements. Figure 10 shows the Raman spectra measured at ambient pressure before and after compression up to 30 GPa. Before compression, the spectrum corresponds to the zircon phase as identified by the presence of ten most intense Raman phonons of the zircon phase indicated by ticks in the figure [63]. After compression,

the spectrum completely changes with eighteen phonons (depicted by ticks in the figure), which is the number of phonons expected for fergusonite phase [64]. Indeed the Raman spectrum of the recovered sample resembles that of a fergusonite, with four modes in the high-frequency region and the remaining fourteen modes at low frequency. The wave numbers of the new eighteen modes are given in table 3, where frequencies of these modes are compared with phonon frequencies of zircon and scheelite phases [63]. We have also calculated the Raman modes for the fergusonite structure. The calculated frequencies and the mode assignment are given in table 3. Calculations predict a similar Raman modes distribution. The agreement between calculated and measured frequencies is within 6% for most of the phonons. The largest discrepancy is 17% for a mode measured at 428 cm^{-1} and calculated to have a wavenumber of 354.87 cm^{-1}. Therefore, calculations confirm the identification of the Raman spectrum measured after decompression to be fergusonite phase. In addition to the Raman modes, the fergusonite structure has fifteen IR optic modes and three acoustic modes. Our calculations also provide information on IR-active modes. Though IR measurements have not been carried out in the present work, we report the results of calculations for the sack of completeness and to allow the comparison with future studies. The mode assignment and wavenumbers of the fifteen IR-active modes are given in table 4. The good agreements reached for the Raman modes between experiments and calculations suggest that present calculations of IR modes could be a good guide for future experiments. DFT calculations have recently described properly the IR modes in related compounds [65].

Summary

To summarise, in this work we have shown, by a combination of experimental and theoretical techniques that non-hydrostatic compression can be used to get a direct phase transformation from zircon to fergusonite in $ScVO_4$. High pressure x-ray diffraction measurements were carried out up to nearly 33 GPa. Results show evidence of an irreversible

zircon to fergusonite phase transition with large pressure region of phase co-existence indicating the nature of transition to be of first order. X-ray diffraction and Raman scattering measurements on pressure retrieved samples confirm the metastability of fergusonite phase. Optical measurements on ambient zircon phase and high pressure fergusonite phase indicates a reduction in the band gap at the phase transition. In addition, there is a marginal blue and red shift of the band gap energy in the low-pressure and high-pressure phases respectively. The experimental findings are well corroborated with first principles calculations. An equation of state for both the phases has been obtained from experiments as well as theory. Ambient pressure bulk modulus for high pressure phase indicates the stiffening of the material compared to ambient zircon phase. Finally, the Raman and IR modes of the novel fergusonite polymorph are identified and their mode symmetry assigned.

Acknowledgments

ABG and DE acknowledge Drs. S. N. Achary and A. K. Tyagi for providing the sample for quench experiments. ABG acknowledges Mr. N. Patel for collecting the XRD data on pressure cycled sample. She also acknowledges the DST, India for travel support and Italian Government for hospitality at Elettra, Italy. This paper was partially supported by the Spanish Ministeriode Economıa y Competitividad (MINECO) under Grants No. MAT2013-46649-C04-01/03-P, MAT2016-75586-C4-1/3-P, and No.MAT2015-71070-REDC (MALTA Consolider).

References

[1] Ekthammathat N, Thongtem T, Phuruangrat A and Teams T 2013 *J. Nanomaterials* **2013** 434197

[2] Martınez-Huerta M V, Coronado J M, Fernandez-Garcia M, Iglesias-Juez A, Deo G, Fierro J L G and Bañares M A 2004 *J. Catal.* **225** 240

[3] Fang Z M, Hong Q, Zhou Z H, Dai S J, Weng W Z and Wan H L 1999 *Catal. Lett.* **61** 39

[4] Maunders E A and DeShazer L G 1971 *J. Opt. Soc. Am.* **61** 684

[5] Bass M 1975 *IEEE J. Quantum Electron.* **11** 938

[6] Jia C J, Sun L D, Luo F, Jiang X C, Wei L H and Yan C H 2004 *Appl. Phys. Lett.* **84** 5305

[7] Liu J F and Li Y D 2007 *Adv. Mater.* **19** 1118

[8] Gu M, Liu Q, Mao S P, Mao D L and Chang C 2008 *Cryst. Growth. Des.* **8** 1422

[9] Lempicki A, Berman E, Wojtowicz A J, Balcerzyk M and Boatner L A 1993 *IEEE Trans. Nucl. Sci.* **40** 384

[10] Wojtowicz A J, Wisniewski D, Lempicki A and Boatner L A 1995 *Radiation Effects and Defects in Solids* (Overseas Publishers Association, Amsterdam)

[11] Deng H, Yang S H, Xiao S, Gong H M and Wang Q Q 2008 *J. Am. Chem. Soc.* **130** 2032

[12] Kaminskii A A, Ueda K, Eichler H J, Kuwano Y, Kouta H, Bagaev S N, Chyba T H, Barnes J C, Gad G M A, Murai T and Li J R 2001 *Opt. Commun.* **194** 201

[13] Kaminskii A A, Lux O, Rhee H, Eichler H J, Ueda K, Oka K and Shibata H 2008 *Appl. Phys.* B **93** 865

[14] Wanmaker W L, Bril A, Ter Vrugt J W and Broos J 1966 *Philips Res. Rep.* **21** 270

[15] Huignard A, Buissette V, Franville A, Gacoin T and Boilot J 2003 *J. Phys. Chem.* B **107** 6754

[16] Hou Z, Yang P, Li C, Wang L, Lian H, Quan Z and Lin J 2008 *Chem. Mater.* **20** 6686

[17] Gehring G A and Gehring K A 1975 *Rep. Prog. Phys.* **38** 1

[18] Popescu C, Garg A B, Errandonea D, Sans J A, Rodriguez-Hernández P, Radescu S, Muñoz A, Achary S N and Tyagi A K 2016 *J. Phys.: Condens. Matter* **28** 035402

[19] Garg A B and Errandonea D, 2015 *J. Solid State Chem.* **226** 147

[20] Garg A B, Errandonea D, Rodríguez-Hernández P, López-Moreno S, Muñoz A and Popescu C 2014 *J. Phys.: Condens. Matter* **26** 265402

[21] Rao R, Garg A B, Sakuntala T, Achary S N and Tyagi A K 2009 *J. Solid State Chem.* **182** 1879

[22] Garg A B, Rao R, Sakuntala T, Wani B N and Vijayakumar V 2009 *J. Appl. Phys.* **106** 063513

[23] Mittal R, Garg A B, Vijayakumar V, Achary S N, Tyagi A K, Godwal B K, Busetto E, Lausi A and Chaplot S L 2008 *J. Phys.: Condens. Matter* **20** 075223

[24] Errandonea D, Achary S N, Pellicer-Porres J, Tyagi A K 2013 *Inorg. Chem.* **52** 5464

[25] Paszkowicz W, Ermakova O, Lopez Solano J, Mujica A, Muñoz A, Minikayev R, Lathe C, Gierlotka S, Nikolaenko I and Dabkowska H 2014 *J. Phys.: Condens. Matter* **26** 025401

[26] Errandonea D, Lacomba-Perales R, Ruiz-Fuertes J, Segura A, Achary S N and Tyagi A K 2009 *Phys. Rev.* B **79** 184104

[27] Nyman H, Hyde B G and Andersson S 1984 *Acta Cryst.* B **40** 441

[28] Errandonea D and Manjón F J 2008 *Prog. Mater. Sci.* **53** 711

[29] Garg A B, Shanavas K V, Wani B N and Sharma S M 2013 *J. Solid State Chem*. **203** 273

[30] Errandonea D, Kumar R S, Achary S N and Tyagi A K 2011 *Phys. Rev.* B **84** 224121

[31] Errandonea D, Popescu C, Achary S N, Tyagi A K and Bettinelli M 2014 *Mater. Res. Bull*. **50** 279

[32] Yuan H, Wang K, Wang C, Zhou B, Yang K, Liu J and Zou B 2015 *The J. Phys. Chem.* C **119** 8364

[33] Ermakova O, Lopez-Solano J, Minikayev R, Carlson S, Kaminska A, Głowacki M, Berkowski M, Mujica A, Muñoz A and Paszkowicz W 2014 *Acta Cryst.* B **70** 533

[34] Errandonea D, Pellicer-Porres J, Martínez-García D, Ruiz-Fuertes J, Friedrich A, Morgenroth W, Popescu C, Rodríguez-Hernández P, Muñoz A and Bettinelli M 2016 *J. Phys. Chem.* C **120** 13749

[35] Panchal V, Errandonea D, Segura A, Rodrıguez-Hernandez P, Muñoz A, Lopez-Moreno S and Bettinelli M 2011 *J. Appl. Phys.* **110** 043723

[36] Errandonea D, Gomis O, García-Domene B, Pellicer-Porres J, Katari V, Achary S N, Tyagi A K and Popescu C 2013 *Inorg. Chem.* **52** 12790

[37] Errandonea D, Muñoz A and Gonzalez-Platas J 2014 *J. Appl. Phys.* **115** 216101

[38] Errandonea D 2015 *Crystal Research and Technology* **50** 729

[39] Chakoumakos B C, Abraham M M and Boatner L A 1994 *J. Solid State Chem.* **109** 197

[40] Dewaele A, Loubeyre P and Mezouar M 2004 *Phys. Rev.* B **70** 094112

[41] Hammersley A P, Svensson S O, Hanfland M, Fitch A N and Häusermann D 1996 *High Pres. Res.* **14** 235

[42] Larson A C and von Dreele R B 2004 *LANL Report* 86–748

[43] Gomis O, Sans J A, Lacomba-Perales R, Errandonea D, Meng Y, Chervin J C and Polian A 2012 *Phys. Rev.* B **86** 054121

[44] Dewaele A, Torrent M, Loubeyre P and Mezouar M 2008 *Phys. Rev.* B **78** 104102

[45] Lacomba-Perales R, Errandonea D, Segura A, Ruiz-Fuertes J, Rodriguez-Hernandez P, Radescu S, Lopez-Solano J and Mujica A 2011 *J. Appl. Phys.* **110** 043703

[46] Errandonea D, Martinez-Garcia D, Lacomba-Perales R, Ruiz-Fuertes J and Segura A 2006 *Appl. Phys. Lett.* **89** 091913

[47] Hohenberg P and Kohn W 1964 *Phys. Rev.* B **135** 864

[48] Kresse G and Furthmüller J 1996 *Comput.Mater.Sci.* **6** 15

[49] Blöchl P E 1994 *Phys. Rev.* B **50** 17953

[50] Perdew J P, Ruzsinszky A, Csonka G I, Vydrow O A, Scuseria G E, Constantin L A, Zhou X and Burke K 2008 *Phys. Rev. Lett*. **100** 136406

[51] Monkhorst H J and Pack J D 1976 *Phys. Rev.* B **13** 5188

[52] López-Solano J, Rodríguez-Hernández P and Muñoz A, 2009 *High Pres. Res.* **29** 582

[53] Parlinski K, Li Z Q and Kawazoe Y 1997 *Phys. Rev. Lett*. **78** 4063

[54] Errandonea D, Meng Y, Somayazulu M, Häusermann D 2005 *Physica* B **355** 116

[55] Birch F 1947 *Phys. Rev*. **71** 809

[56] Klotz S, Chervin J C, Munsch P and Marchand G Le 2009 *J. Phys. D: Appl. Phys.* **42** 075413

[57] Yue B, Hong F, Merkel S, Tan D, Yan J, Chen B and Mao H K 2016 *Phys. Rev. Lett.* **117** 135701

[58] Gleissner J, Errandonea D, Segura A, Pellicer-Porres J, Hakeem M A, Proctor J E, Raju S V, Kumar R S, Rodríguez-Hernández P, Muñoz A, Lopez-Moreno S and Bettinelli M 2016 *Phys. Rev.* B **94** to appear

[59] Errandonea D, Muñoz A, Rodríguez-Hernández P, Proctor J E, Sapiña F and Bettinelli M 2015 *Inorg. Chem.* **54** 7524

[60] Dolgos M R, Paraskos A M, Stoltzfus M W, Yarnell S C and Woodward P M 2009 *J. Solid State Chem.* **182** 1964

[61] Cong H, Zhang H, Yao B, Yu W, Zhao X, Wang J and Zhang G 2010 *Cryst. Growth Des.***10** 4389

[62] Yuldashev Sh U, Igamberdiev Kh T, Kwon Y H, Lee S, Liu X, Furdyna J K, Shashkov A G and Kang T W 2012 *Phys. Rev.* B **86** 125202

[63] Panchal V, Manjon F J, Errandonea D, Rodriguez-Hernandez P, Lopez-Solano J, Muñoz A, Achary S N and Tyagi A K 2011 *Phys. Rev.* B **83** 064111

[64] Botella P, Lacomba-Perales R, Errandonea D, Polian A, Rodríguez-Hernández P and Muñoz A 2014 *Inorg. Chem.* **53** 9729

[65] Errandonea D, Muñoz A, Rodríguez-Hernández P, Gomis O, Achary S N, Popescu C, Patwe S J and Tyagi A K 2016 *Inorg. Chem.* **55** 4958

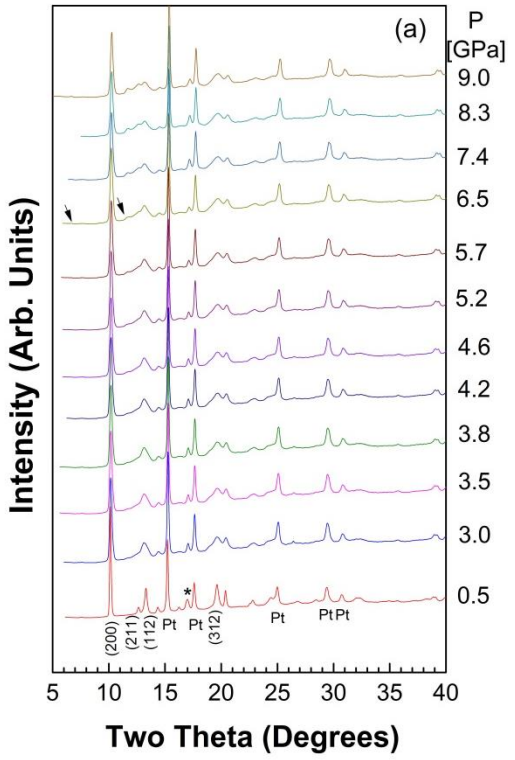

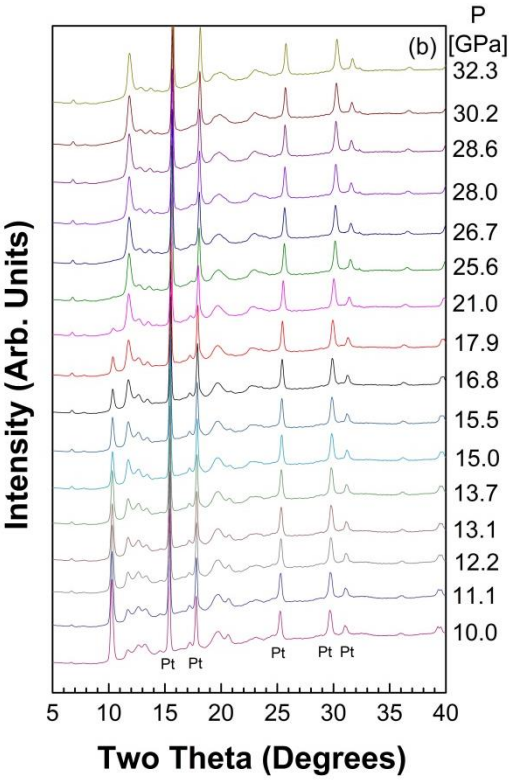

Figure 1: continue in next page.

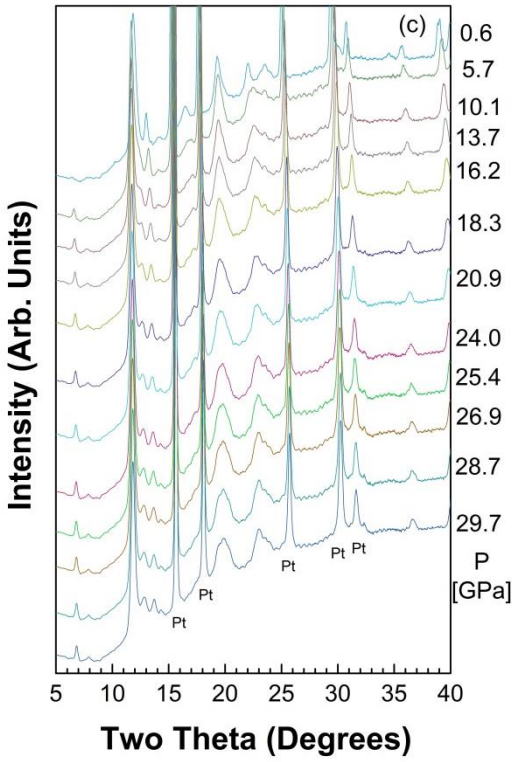

Figure 1: Evolution of diffraction peaks with (a and b) increasing pressure and (c) pressure unloading. Arrow indicates the appearance of new diffraction peaks. Pressures are indicated in GPa. Pt shows the platinum peaks. Some peaks of the zircon structure have been labelled.

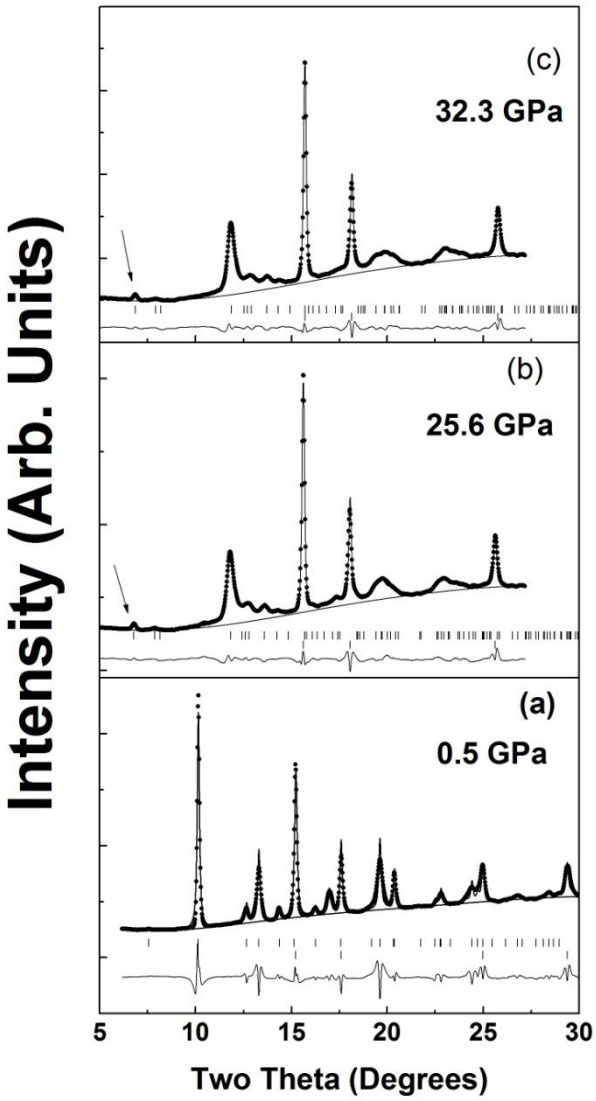

Figure 2: (a) Rietveld refined data at 0.5 GPa, (b) at 25.6 GPa and (c) at 32.3 GPa. Upper tick marks are for the sample reflection and lower tick mark for the Pt pressure standard. Arrows in figure b and c indicates the (020) reflection of the fergusonite phase.

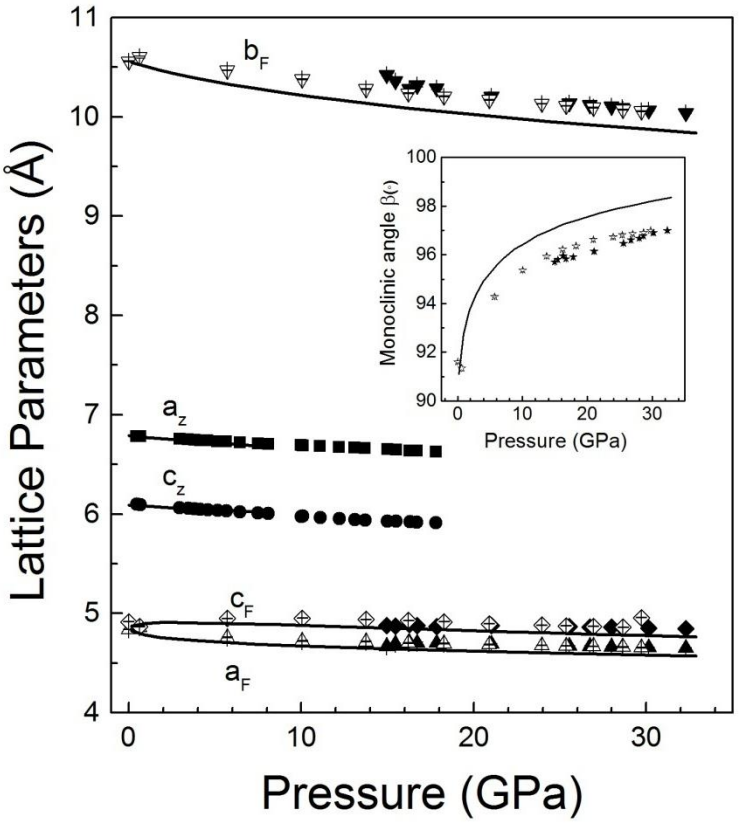

Figure 3: Unit cell parameters for ambient zircon phase and high pressure fergusonite phase. Error bars have also been plotted for all the data points. Symbols a_z and c_z refers to *a* and *c* parameters for zircon phase while a_F, b_F and c_F represent *a*, *b* and *c* axis parameters for the fergusonite phase with solid symbols for pressure loading and corresponding open symbols are while unloading the pressure. Inset of the figure shows the changes in the monoclinic angle β, solid stars increasing pressure, open stars decreasing pressure. Solid lines correspond to theoretical calculations.

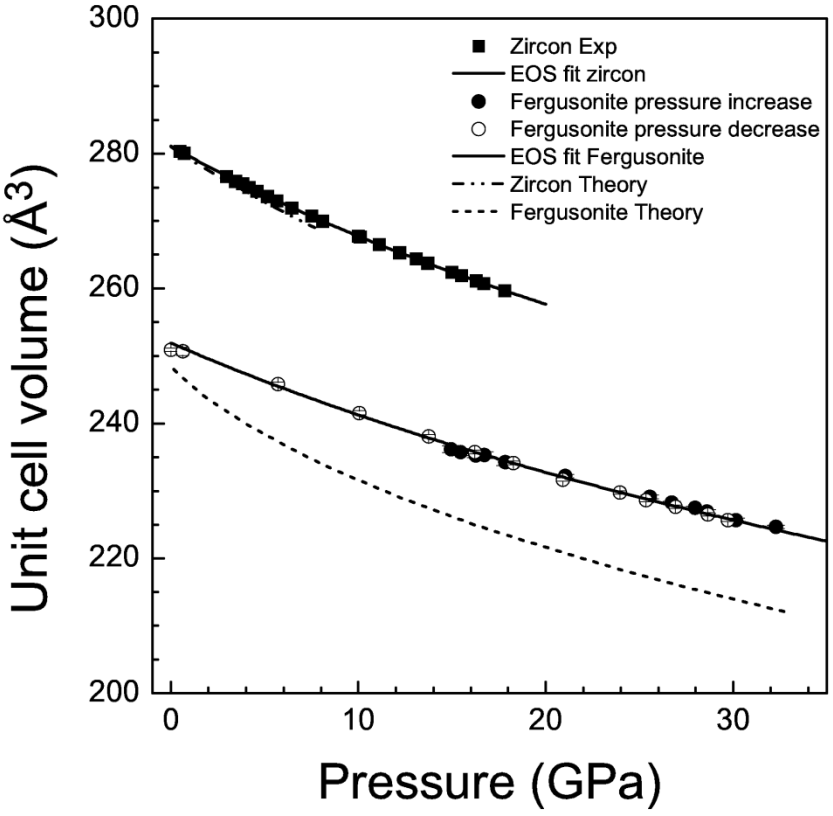

Figure 4: Pressure volume data for zircon and fergusonite phase. Symbols have been explained in the figure.

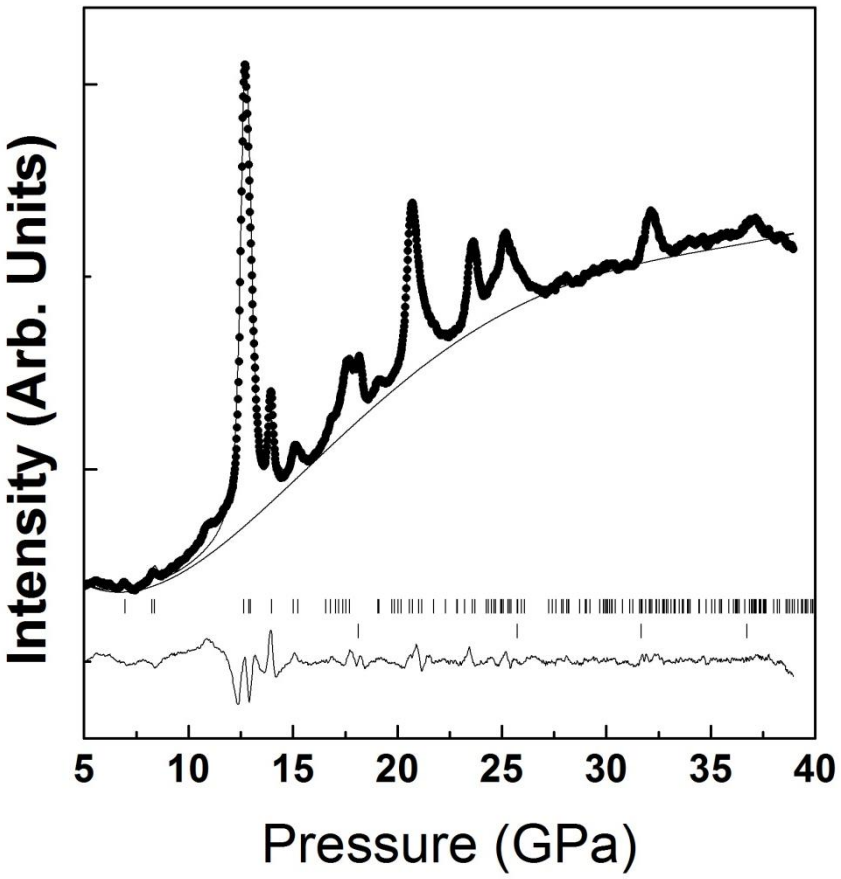

Figure 5: X-ray diffraction data collected on pressure retrieved sample. Lower tick marks are reflection from the sample chamber.

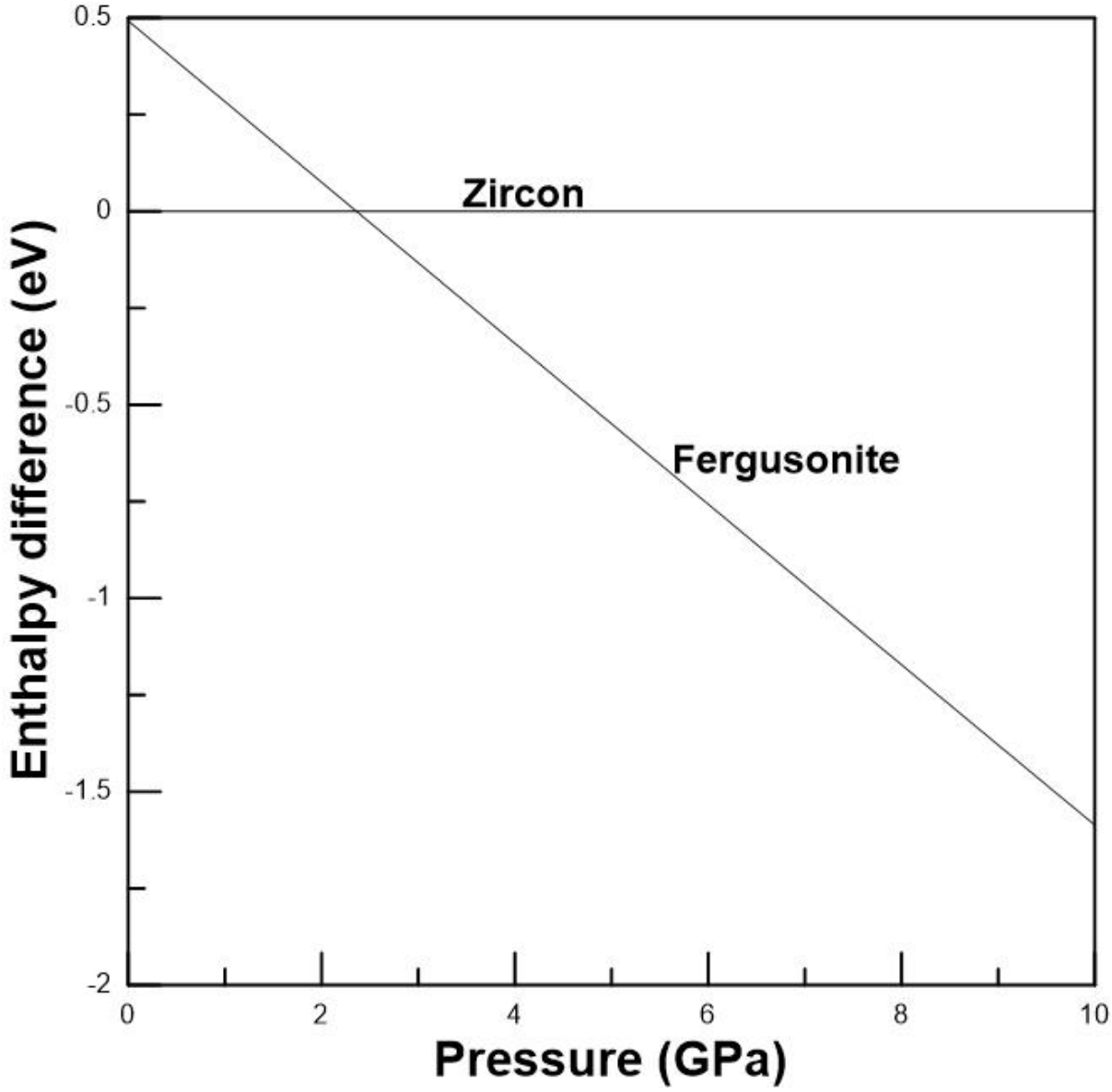

Figure 6: Enthalpy difference as a function of pressure showing the phase transition reported here. The zircon phase has been taken as reference.

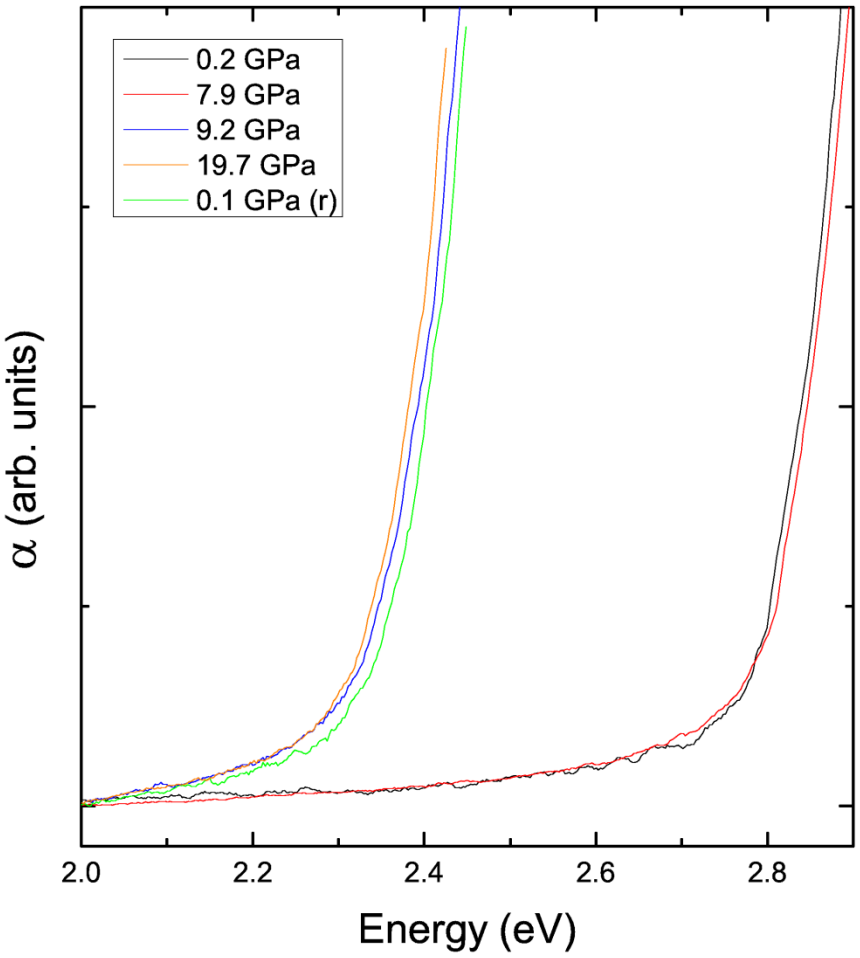

Figure 7: Optical-absorption spectra of $ScVO_4$ at different pressures. The measurement labelled as 0.1(r) correspond to the experiment carried out after decompression.

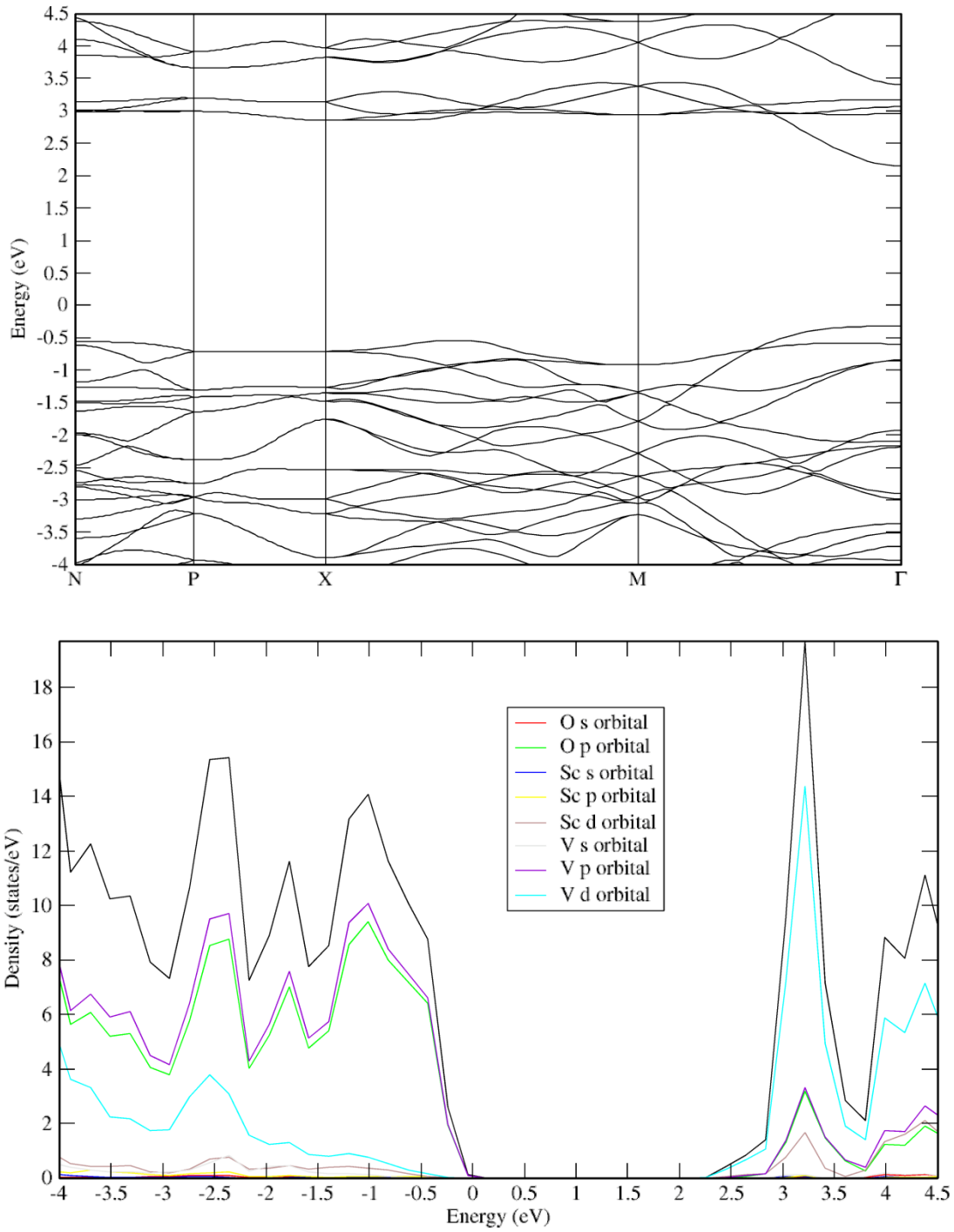

Figure 8: Band structure and density of states of zircon-type $ScVO_4$ at ambient pressure.

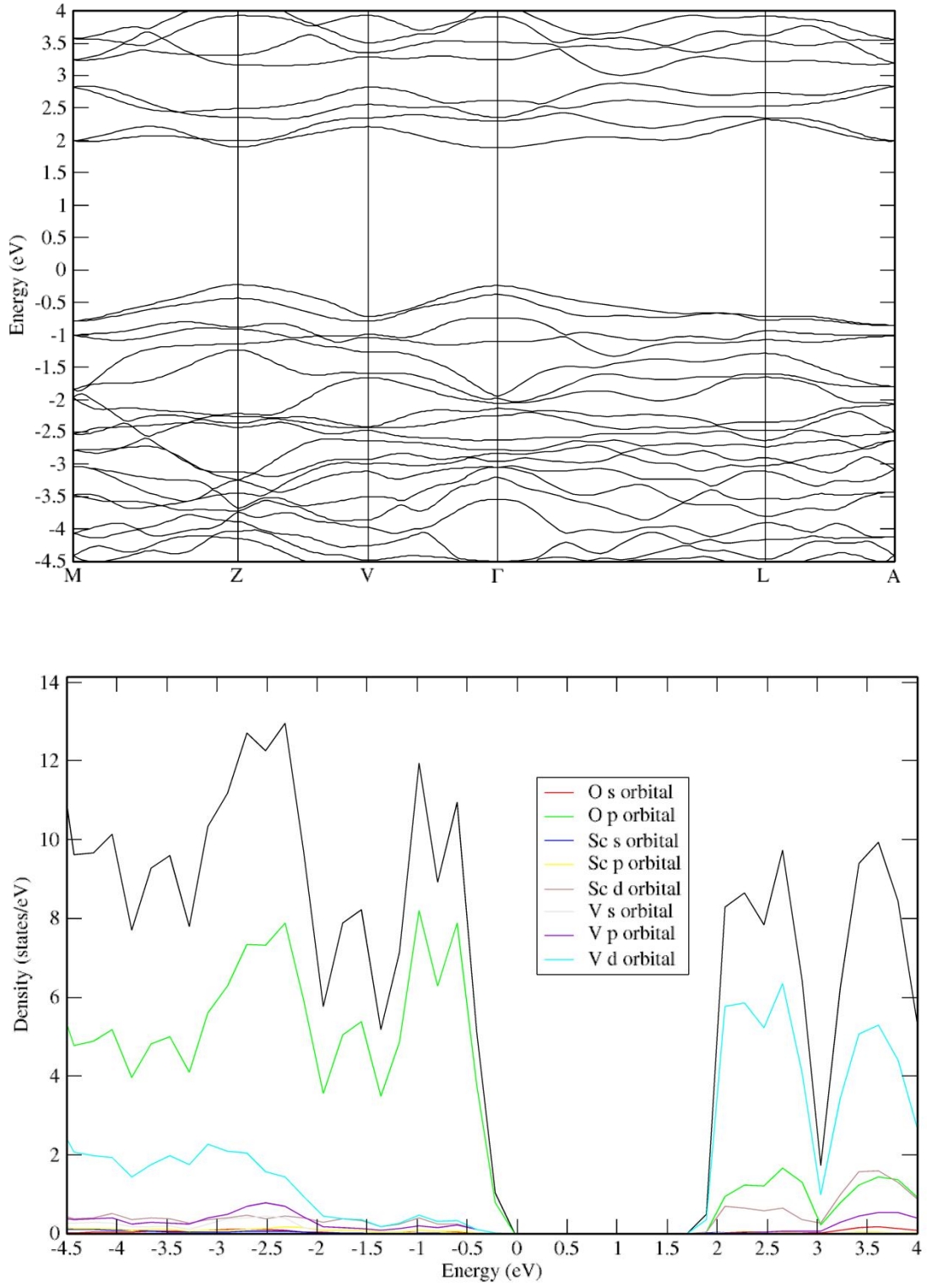

Figure 9: Band structure and density of states of fergusonite-type $ScVO_4$ at ambient pressure.

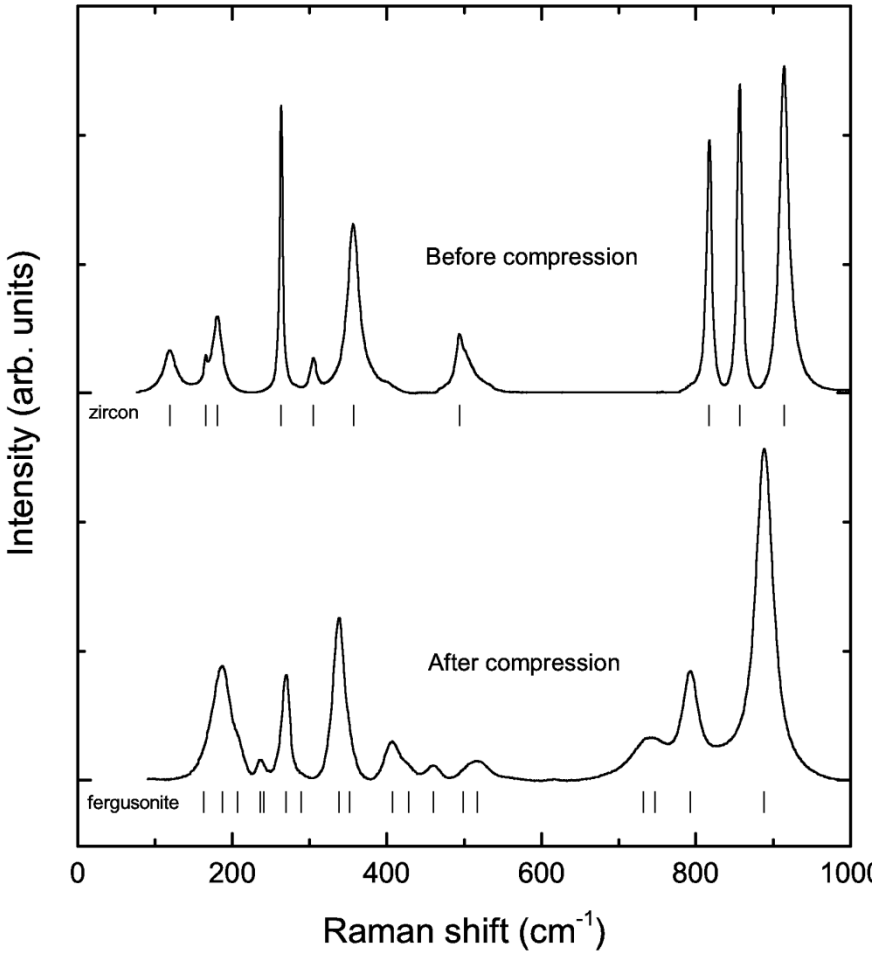

Figure 10: Raman spectra of $ScVO_4$ measured at ambient pressure before and after pressure cycled sample from 30 GPa.

Table 1: Refined atomic positions for zircon (top), fergusonite (middle), metastable fergusonite (bottom) $ScVO_4$ at 0.5, 25.6 GPa and ambient pressure respectively.

Atom	Site	x	y	z
Sc	4a	0	3/4	1/8
V	4b	0	1/4	3/8
O	16h	0	0.4250(15)	0.1845(24)
Sc	4e	1/4	0.6229(11)	0
V	4e	1/4	0.1477(9)	0
O	8f	0.003(12)	0.9542(17)	0.298(5)
O	8f	0.570(11)	0.2104(20)	0.792(9)
Sc	4e	1/4	0.6236(22)	0
V	4e	1/4	0.1397(23)	0
O	8f	0.060(11)	0.9538(13)	0.305(8)
O	8f	0.577(6)	0.2077(17)	0.828(7)

Table 2: Calculated atomic positions for different atoms in fergusonite $ScVO_4$ at ambient pressure: a = 4.78307 Å, b = 10.51057 Å, c = 4.89893 Å, and β = 92.7476º.

Atom	Site	x	y	z
Sc	4e	1/4	0.62662	0
V	4e	1/4	0.13515	0
O	8f	0.09453	0.95683	0.25904
O	8f	0.51299	0.21020	0.87749

Table 3: Raman modes of fergusonite $ScVO_4$ at ambient pressure wavenumbers are in cm^{-1}. For comparison we also show the Raman frequencies of zircon and scheelite phases. The relative difference between measured and calculated wavenumbers was done taking the experimental result as the reference value.

Mode	Fergusonite Theory This work	Fergusonite Experiments This work	Relative difference between theory and experiment in %	Scheelite from [56]	Zircon from [56]
A_g	166.62	163	-2.22	177.5	119.3
B_g	181.76	187	2.80	207.8	165.6
B_g	193.73	207	6.41	222.5	180.5
B_g	225.45	236	4.47	239.6	263.2
A_g	232.26	241	3.63	318.7	304.8
B_g	241.37	269	10.27	330.4	356.7
A_g	247.90	289	14.22	338.2	494.1
A_g	322.09	338	4.71	425.3	817.1
B_g	338.57	352	3.82	425.7	856.5
A_g	354.44	407	12.91	755.8	914.2
B_g	354.87	428	17.09	793.9	
A_g	433.16	460	5.83	809.3	
B_g	434.83	499	12.86		
B_g	441.34	517	14.63		
B_g	768.93	732	-5.05		
B_g	788.71	747	-5.58		
A_g	801.92	793	-1.12		
A_g	837.15	888	5.73		

Table 4: IR modes of fergusonite $ScVO_4$ at ambient pressure, wavenumbers are in cm^{-1}.

Mode	wavenumber	Mode	wavenumber
B_u	167.02	B_u	347.24
A_u	175.45	A_u	484.27
B_u	189.20	A_u	523.56
B_u	254.68	A_u	723.53
B_u	258.81	B_u	725.07
A_u	260.013	B_u	752.12
A_u	309.58	A_u	805.26
B_u	328.49		

Figure captions

Figure 1: Evolution of diffraction peaks with (a and b) increasing pressure and (c) pressure unloading. Arrow indicates the appearance of new diffraction peaks. Pressures are indicated in GPa. Pt shows the platinum peaks. Some peaks of the zircon structure have been labelled.

Figure 2: (a) Rietveld refined data at 0.5 GPa, (b) at 25.6 GPa and (c) 32.3 GPa. Upper tick marks for the sample reflection and lower tick mark are for the Pt pressure standard. Arrows in figure b and c indicates the (020) reflection of the fergusonite phase.

Figure 3: Unit cell parameters for ambient zircon phase and high pressure fergusonite phase. Error bars have also been plotted for all the data points. Symbol a_z and c_z refers to *a* and *c* parameters for zircon phase while a_F, b_F and c_F represent *a*, *b* and *c* axis parameters for the fergusonite phase with solid symbols for pressure loading and corresponding open symbols are while unloading the pressure. Inset of the figure shows the changes in the monoclinic angle β, solid stars increasing pressure, open stars decreasing pressure. Solid lines correspond to theoretical calculations.

Figure 4: Pressure volume data for zircon and fergusonite phase. Symbol has been explained in the figure.

Figure 5: X-ray diffraction data collected on pressure retrieved sample. Lower tick marks are reflection from the sample chamber.

Figure 6: Enthalpy difference as a function of pressure showing the phase transition reported here. The zircon phase has been taken as reference.

Figure 7: Optical-absorption spectra of $ScVO_4$ at different pressures. The measurement labelled as 0.1(r) correspond to the experiment carried out after decompression.

Figure 8: Band structure and density of states of zircon-type $ScVO_4$ at ambient pressure.

Figure 9: Band structure and density of states of fergusonite-type $ScVO_4$ at ambient pressure.

Figure 10: Raman spectra of $ScVO_4$ measured at ambient pressure before and after pressure cycled sample from 30 GPa.

Table Captions

Table 1 Refined atomic positions for zircon (top), fergusonite (middle), metastable fergusonite (bottom) $ScVO_4$ at 0.5, 25.6 GPa and ambient pressure respectively.

Table 2 Calculated atomic positions for different atoms in fergusonite $ScVO_4$ at ambient pressure: a = 4.78307 Å, b = 10.51057 Å, c = 4.89893 Å, and β = 92.7476º.

Table 3 Raman modes of fergusonite $ScVO_4$at ambient pressure wavenumbers are in cm^{-1}. For comparison we also show the Raman frequencies of zircon and scheelite phases. The relative difference between measured and calculated wavenumbers was done taking the experimental result as the reference value.

Table 4 IR modes of fergusonite $ScVO_4$ at ambient pressure, wavenumbers are in cm^{-1}.